Near-Infrared Spectroscopic Study of Secondary Mineral in the Oxidation Zones of Copper-Bearing Deposits

Wu Shao-kun , He Ming-yue * , Yang Mei , Peng Bi-jie , Shi Yu-jia , Sun Kai-yue

Posted Date: 29 July 2024

doi: 10.20944/preprints202407.2241.v1

Keywords: dioptase; malachite; azurite; near-infrared spectroscopy; combination vibrations

Article

Near-Infrared Spectroscopic Study of Secondary Mineral in the Oxidation Zones of Copper-Bearing Deposits

Wu Shao-kun [1], He Ming-yue [1,*], Yang Mei [2], Peng Bi-jie [1], Shi Yujia [1] and Sun kaiyue [1]

[1] Gemological Institute of China University of Geosciences, Beijing 10008; 3009210005@cugb.com (W. S.); 2024700015@cugb.com (P. B.); 3009220006@ cugb.edu.cn (Y. S.); 3009210004@email.cugb.edu.cn (S. K.)
[2] Sciences Institute of China University of Geosciences, Beijing 100083; yangmei@cugb.edu.cn
* Correspondence: hemy@cugb.edu.cn

Abstract: This study measured the infrared spectra of secondary minerals in the oxidation zones of three types of copper ores: dioptase, malachite, and azurite, and detailedly assigned the peak positions of OH stretching vibrations and the origins of OH combination vibrations. Dioptase contains three types of water molecules with different orientations within its ring channels, which exhibit six kinds of OH stretching vibrations in the 3000-3600 cm^{-1} range, the bond length range is 2.652-2.887 Å. Among them, the 3443 cm^{-1} band shows strong near-infrared activity and combines with Si-O vibrations or OH bending vibrations in the structure, resulting in five combination vibration peaks in the 4000-5000 cm^{-1} range. Malachite contains two inequivalent hydroxyls in its structure, leading to two OH stretching vibrations in the high-frequency region, located at 3314 and 3402 cm^{-1}, respectively. Azurite contains only one type of hydroxyl, thus only one characteristic OH stretching vibration is present, at 3424 cm^{-1}. The OH stretching vibrations of malachite and azurite mainly combine with $[CO_3]^{2-}$ vibrations or OH bending vibrations, leading to six and five combination peaks in the OH combination vibration region, respectively. By analyzing the combination of peak positions at 4341 cm^{-1} in the near-infrared spectrum, the merged OH bending vibration at 921 cm^{-1} in azurite was discovered. Spectroscopic research on secondary minerals can better provide a basis for ore exploration and geological remote sensing.

Keywords: dioptase; malachite; azurite; near-infrared spectroscopy; combination vibrations

1. Introduction

Copper is one of the earliest metals utilized by humans and continues to play an irreplaceable role in modern human society. Copper ores come in various types, such as porphyry, skarn, and shale, among others [1]. The characteristics and scales of these different types of deposits are highly complex. Utilizing secondary copper minerals in the oxidation zone for exploration is an effective method of prospecting. Typically, in the upper oxidation zone of copper ore deposits, minerals such as cuprite, chalcopyrite, azurite, and malachite are found, which can coexist and transform into each other under certain conditions. They typically exhibit vivid colors, making them easily identifiable. They also inherit the geochemical characteristics of the original deposits [2]. These minerals are also commonly used in pigments and are frequently encountered in archaeology and material science. Those with good form and color can also be used as gemstones or mineral specimens.

Dioptase [$Cu_6(Si_6O_{18})\cdot 6H_2O$] is a copper silicate hydroxide with six-membered (Si_6O_{18}) rings. It is almost exclusively restricted in its occurrence to the oxidation zones of copper-bearing deposits in arid climates. Its ring structure is composed of six silicate tetrahedra that fold into a triangular ring, with the six water molecules forming a distorted version of this ring [3]. These water molecules are situated within the silicate ring structure, which is coordinated by copper atoms both laterally and longitudinally [4].

 doi:10.20944/preprints202407.2241.v1

Spectroscopy is an invaluable tool for investigating the crystal structures of minerals. Changes observed in infrared and Raman spectroscopy indicate that the crystal structure of diopside remains largely unchanged at 600 °C [4–6] or under pressures of 14.5 GPa [7,8]. This suggests that diopside has a high degree of stability. The gradual loss of water molecules within the channels over a broad temperature range as the temperature increases is also noteworthy. The study of Ruan [9] of infrared and Raman spectroscopic on diopside from Namibia and the Democratic Republic of the Congo revealed that the vibrational frequencies of the ring anions increase with the widening of the Si-O-Si bond angles. As a result, variations in composition can lead to minor changes in the crystal structure framework, which in turn cause shifts in the frequency and intensity of the spectral bands that reflect the crystal structure framework. This characteristic can be exploited to discern compositional differences through spectral variations, thus differentiating the environmental conditions under which the mineral formed.

Malachite [$Cu_2(CO_3)(OH)_2$] and azurite [$Cu_3(CO_3)_2(OH)_2$] are two fundamental copper carbonate minerals characterized by their chain-like structures. The [CO_3] groups form these chain structures by coordinating with cations and (OH) polyhedra. Current spectroscopic research on malachite and azurite predominantly focuses on Raman spectroscopy [10–12], which allows for a detailed assignment of Raman bands to the corresponding vibration groups. Xu [13] and colleagues also studied the Raman spectral changes of azurite under high pressure at room temperature, providing insights into the behavior of hydroxide under extreme conditions. Schuiskii [14] conducted an infrared spectroscopic study of natural and synthetic malachite in the range of 400-4000 cm^{-1}, meticulously assigning the peaks to their respective vibration groups. However, there is still a relative scarcity of research on infrared, especially near-infrared, spectroscopy for these minerals.

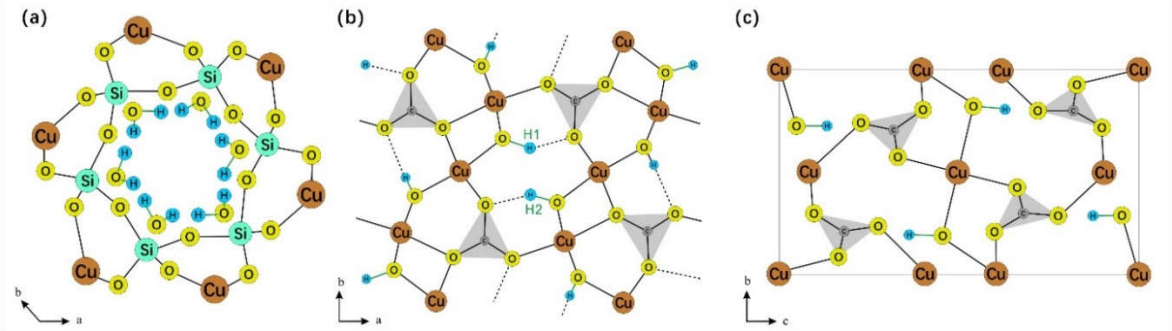

Figure 1. (a) The silicate ring structure and internal water molecules of dioptase. Note that water molecules and silica ring are not in the same plane (modified according to Ribbe [3]); (b) The crystal structure of malachite, in which there are two kinds of hydroxyl groups (modified according to Süsse [15]); (c) The crystal structure of azurite (modified according to Belokoneva [16]). O-H bonds in three mineral structures are marked in green.

This study investigates the mid-infrared(MIR) and near-infrared(NIR) spectra of three copper minerals. The findings are applicable to the identification and research of minerals and archaeology. Additionally, the correlation between mid-infrared and near-infrared spectra is an intriguing area of study. The research also provides a detailed discussion on the assignment and attribution of the OH vibrational spectral peaks in the near-infrared region, attempting to rationalize the origins of these composite bands. Careful measurement and interpretation of the infrared spectra of secondary copper minerals may be crucial for mineral exploration, research, and the interpretation of geological remote sensing data.

2. Materials and Methods

The samples were sourced from the National Mineral Rock and Fossil Resource Center (NIMRF) of China (Figure 2). The dioptase is a single crystal originating from the Tsumeb region in Namibia, exhibiting an idiomorphic rhombohedral form. Malachite and azurite are aggregates, collected from

 doi:10.20944/preprints202407.2241.v1

the Daye area in Hubei, China. Azurite forms sphere with columnar single crystals visible under magnification; malachite crystals are fibrous and have an overall crustaceous structure.

Isomorphism commonly occurs in minerals, and impurity elements can affect the results of spectroscopic experiments to varying degrees. Before this study, the samples were analyzed using micro-area X-ray fluorescence (XRF), and the results indicated that the samples generally contain elements such as Al, Fe, Ca, Cl, etc., with generally low concentrations (Table 1). The azurite sample contains higher amounts of silicon and aluminum, which may be due to the azurite sample being an aggregate with a small amount of country rock or inclusions mixed in. Before test, the samples are pulverized and purified under a microscope to ensure the accuracy of the spectra.

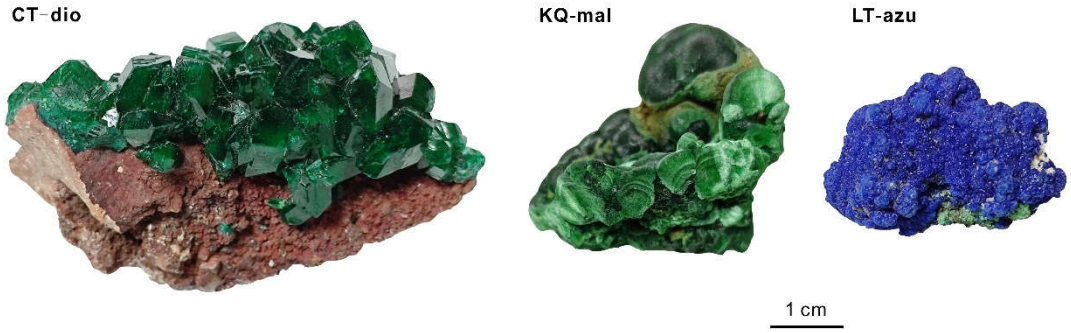

Figure 2. Sample characteristic of copper minerals in the oxidation zones.

Table 1. Mineral composition of the samples.

Sample	Color	Minerals	SG	Isomorphism (w%)
CT-dio	Green	Dioptase	3.32	Mg-0.21%, Al-0.51%, Ca-0.14%, Fe-0.04%, S-0.17%, Cl-0.53%
KQ-mal	Green	Malachite	4.22	Mg-0.02%, Mn-0.01%, Ca-0.02%, Fe-0.01%, Si-0.20%, Cl-0.09%
LT-azu	Blue	Azurite	3.84	K-0.49%, Al-1.35%, Ca-0.11%, Fe-0.14%, Si-3.16%, Ti-0.06%

Fourier transform infrared spectroscopy (FTIR) measurements were performed at room temperature, using the Bruker Tensor II spectrometer at the laboratory of NIMRF. The spectra were collected in transmission mode in a tablet of KBr. The mid-infrared scanning range was 400~4000 cm^{-1} with a resolution of 4 cm^{-1}. The near-infrared scanning range was 4000~8000 cm^{-1}, with a resolution of 8 cm^{-1}. Each spectrum was averaged from 64 scans to improve the signal-to-noise ratio. If the mineral particles size is larger than or close to the infrared wavelength, the infrared light will be affected by multiple scattering within the particles, resulting in an interference effect that reduces the signal strength [17,18]. In this study, the ratio of sample to KBr was increased to enhance the signal and achieve satisfactory results.

3. Results

3.1. Characteristics of MIR

The sample exhibits four main absorption region, specifically at 400-600, 700-1200, 1200-1700, and 3000-3600 cm^{-1}. The spectrum closely matches the characteristic spectra of the corresponding minerals (Figure 3), with no other phases present.

The 3000-3600 cm^{-1} region corresponds to the O-H stretching vibration area. Due to the superposition of multiple spectral peaks, the shape of the spectrum is relatively complex. Therefore,

 doi:10.20944/preprints202407.2241.v1

peak fitting was performed to determine the accurate number and position of spectral peaks, as shown in Figure 4. The peak fitting process utilized the Peakfit v4.12 software, employing a combination of Gauss + Lorentz Area functions, with a correlation coefficient $r^2 > 0.98$ between the fitting function and the original function. The fitting results were verified and calibrated using the second derivative [19–21].

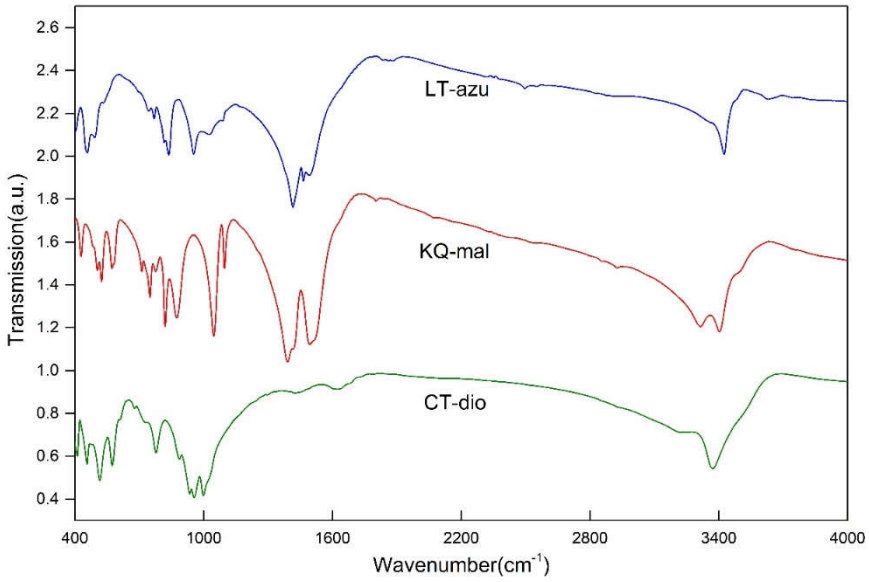

Figure 3. MIR spectrum of copper mineral samples.

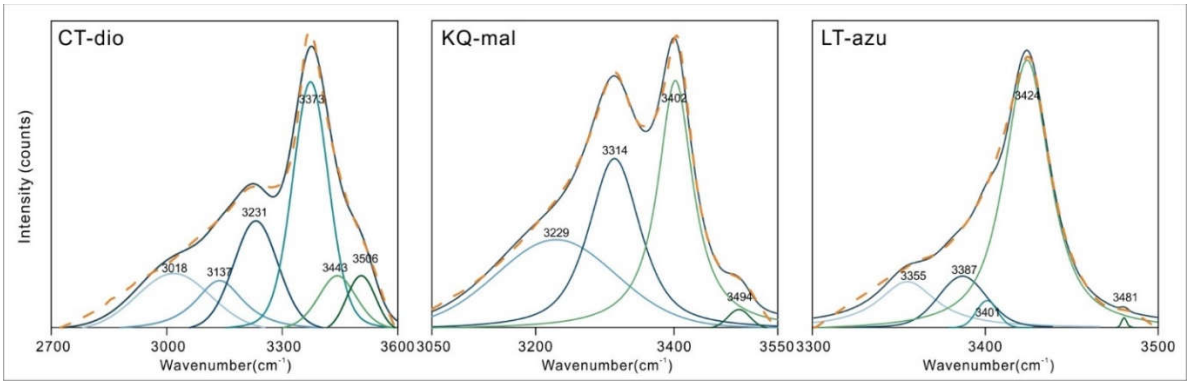

Figure 4. MIR spectral fitted analysis of the OH stretching region. The yellow dashed line represents the original spectrum.

Dioptase in this region exhibits six characteristic peaks, with the strongest absorption located at 3373 cm^{-1}. Frost [4] attributes all peaks are assigned to stretching vibrations of water in silicate rings. The different vibrational frequencies are due to the varying distances between the O-O and H-O bonds [22–26]. He tested the OH stretching vibration position and calculated the corresponding hydrogen bond distance of dioptase from different origins. In this paper, the OH stretching vibration peak position and hydrogen bond distance were fitted:

$$y = 0.0000006424\ x^2 - 0.00371\ x + 7.99784 \quad (1)$$

Where x is the OH stretching vibration peak position, y is the corresponding hydrogen bond distance (Å), r^2=0.941. According to the regression equation, the hydrogen bond distance corresponding to OH stretching vibration of dioptase in this paper is calculated. The bond length range is 2.652-2.887 Å. see Table 2 for the specific distribution.

Malachite shows four peaks in this region, with the main absorptions located at 3314 and 3402 cm^{-1}. In the structure of malachite, there are two inequivalent hydroxyl groups with bond lengths of

 doi:10.20944/preprints202407.2241.v1

0.92 ± 0.2 Å and 1.05 ± 0.14 Å [15]. Due to the increased bond length, the frequency of the stretching vibrations decreases, and the wavenumber correspondingly decreases. Thus, the peak at 3314 cm^{-1} in malachite is assigned to the OH2 stretching vibration, and the peak at 3402 cm^{-1} is assigned to the OH1 stretching vibration. The remaining two peaks located at 3229 and 3494 cm^{-1} are attributed to the stretching vibrations of adsorbed water and the M-OH stretching vibrations caused by isomorphous substitution, as these two positions do not always exhibit characteristic peaks in other studies, or the shift and intensity of the absorption peaks near these positions vary significantly with different samples. Azurite contains only one type of hydroxyl group [16], and therefore the peak at 3424 cm^{-1} is assigned to the OH stretching vibration, with the remaining peaks also considered to be stretching vibrations of adsorbed water or M-OH. The specific assignments of the peak positions are shown in Table 2.

Table 2. The MIR bands of copper mineral samples and their assignments. (cm^{-1}).

Band assignment [4–6,9,27,28]	CT-dio	Band assignment [10,14,29–31]	KQ-mal	Band assignment [10,31]	LT-azu
M-O vibration, Si-O ring bending vibration and both coupled vibration	411 456	Lattice modes Cu-X Stretch	428		
O-Si-O bending vibration	516 574 608 677 778	Lattice modes Cu-OH Stretch	485 524	Lattice modes Cu-OH Stretch	458 532
Si-O stretching vibration	886 934 955 997 1024	Lattice modes Cu-O Stretch	505 572 582	Lattice modes Cu-O Stretch	492
		Outer [CO_3] stretching vibration ν4	713 750	[CO_3] stretching vibration ν4	744 768
		[CO_3] bending vibration	776		
		[CO_3] symmetric stretching vibration ν2	820	[CO_3] symmetric stretching vibration ν2	817
		OH bending vibration	874 1047	OH bending vibration	921* 953 1026
		[CO_3] stretching vibration ν1	1096	[CO_3] stretching vibration ν1	1089
OH (H2O) bending vibration	1425 1492 1620 1641 1681	[CO_3] antisymmetric stretching vibration ν3	1391 1418 1494 1519	[CO_3] antisymmetric stretching vibration ν3	837 1415 1464 1492
OH (H2O) stretching vibration (2.652)	3018	OH (H2O) stretching vibration	3229	OH (H2O) stretching vibration	3355
OH (H2O) stretching vibration (2.681)	3137	OH2 stretching vibration	3314	OH (H2O) stretching vibration	3387
OH (H2O) stretching vibration (2.717)	3231	OH1 stretching vibration	3402	OH (H2O) stretching vibration	3401
OH (H2O) stretching vibration (2.793)	3373	M-OH(no Cu) stretching vibration	3494	OH stretching vibration	3424

 doi:10.20944/preprints202407.2241.v1

OH (H2O) stretching vibration (2.839)	3443	M-OH(no Cu) stretching vibration	3481
OH (H2O) stretching vibration (2.887)	3506		

The corresponding hydrogen bond length (Å) is in brackets, the calculated value is from frost (2013). * not observed in the spectrum directly. See the analysis below for specific reasons.

3.2. Characteristics of NIR

As depicted in Figure 5(a), the near-infrared spectra of the three minerals primarily exhibit absorption bands in the 4000-5200 cm^{-1} region, which are attributed to the combination of hydroxyl stretching vibrations and other vibrational absorptions. The spectral characteristics in the near-infrared region are not pronounced, with only azurite showing two discernible characteristic infrared peaks at 4241 and 4372 cm^{-1}. To further identify the peak positions, the spectra were subjected to baseline correction and normalization, as illustrated in Figure 5(b). Both malachite and azurite display two main absorption bands, occurring within the ranges of 4000-4300 and 4300-4500 cm^{-1}, respectively. The characteristic bands of dioptase are considerably broader compared to the former two, with two main characteristic bands located in the ranges of 4000-4500 and 4500-5200 cm^{-1}. The fitting results present more detailed outcomes (as shown in Figure 6), where the three minerals consist of 5-7 bands in the respective regions, with specific peak positions detailed in Table 3. Malachite and dioptase exhibit a multitude of weak absorption peaks in the 7000-8000 cm^{-1} range, which are attributed to the overtone peaks of hydroxyl or water molecule stretching vibrations associated with vibration groups [32,33].

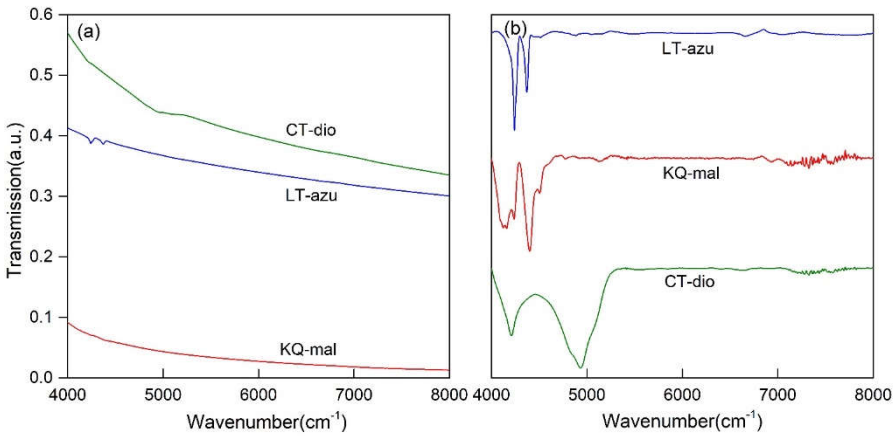

Figure 5. NIR spectrum of copper minerals in the oxidation zones of copper-bearing deposits.

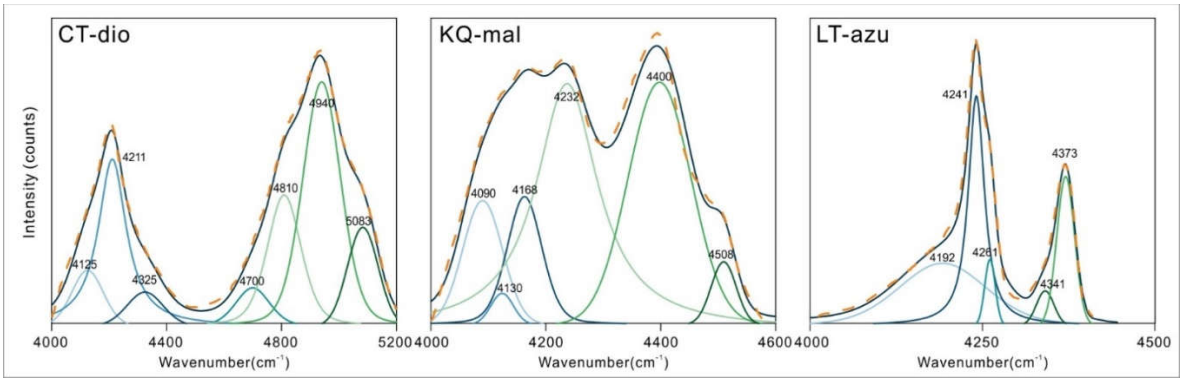

Figure 6. NIR spectral fitted analysis of the OH combination bands. The yellow dashed line represents the original spectrum.

 doi:10.20944/preprints202407.2241.v1

Table 3. The NIR bands of copper minerals in the oxidized zone (cm^{-1}).

CT-dio	KQ-mal	LT-azu
4125	4090	4192
4211	4130	4241
4325	4168	4261
4700	4232	4341
4810	4400	4373
4940	4508	
5083		

4. Discussion

Assignment of OH Vibration in NIR Spectra

The combination vibration region of OH is the primary region for near-infrared signals. The relationship between the bandwidths of near-infrared and mid-infrared spectra is determined through trial calculations and the summation of errors. By combining the data analysis of this experiment, we aim to identify the most suitable near-infrared peak assignments, with specific combinations detailed in Table 4, and the combination error is controlled within 10 cm^{-1} [34,35].

The signals of dioptase in the 4000-5200 cm^{-1} region correspond to the combination of OH stretching vibrations with the vibrations of the siloxane framework or OH bending vibrations. The most combined with the vibrations of the siloxane framework and the bending vibrations of channel water molecules is the band at 3443 cm^{-1}, rather than the strongest at 3373 cm^{-1}. It is speculated that the orientation of the water molecule stretching vibration corresponding to 3443 cm^{-1} is significantly different from other water molecule stretching vibrations [3], leading to an easy formation of a union with other bands.

Malachite exhibits six bands in the 4000-4600 cm^{-1} region, which belong to the combination of two types of OH stretching vibrations and three $[CO_3]^{2-}$ vibrations, with water molecules and the stretching vibrations of M-OH from non-copper ions not participating in the combination vibrations. Among the four bands with higher wavenumbers, the errors between the theoretical and measured values can offset each other, which is considered to be due to the relative shift of the bands caused by mutual influence between the vibrations. In the crystal structure of azurite, only one type of hydroxyl group exists, and all the combination vibrations in the near-infrared region are related to the OH stretching vibration at the position of 3424 cm^{-1}. In addition to the $[CO_3]^{2-}$ vibrations, combinations of hydroxyl stretching and bending vibrations are also observed.

It is worth noting that, based on the calculation of the OH stretching vibration at 3424 cm^{-1} and the combination vibration at 4341 cm^{-1}, there should be an absorption vibration near 917 cm^{-1}. Upon detailed analysis of the nearby spectrum, a corresponding spectrum at 921 cm^{-1} was observed, which the author attributes to the OH bending vibration, as shown in Figure 7, and which has both infrared and Raman activity [6]. This spectral band has hardly been mentioned in previous studies.

 doi:10.20944/preprints202407.2241.v1

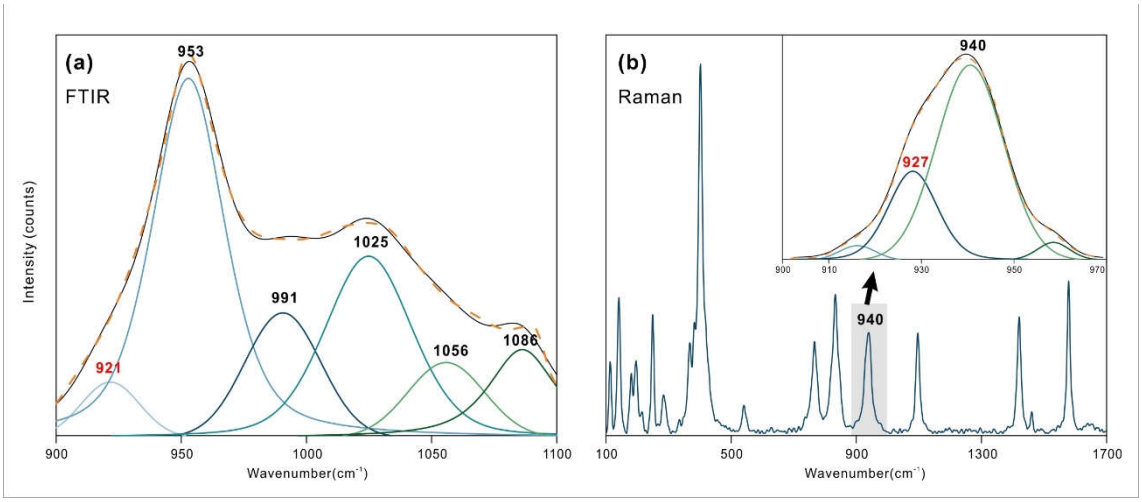

Figure 7. (a) Fitted analysis of infrared hydroxyl bending vibration region of azurite; (b) The Raman spectra of azurite and the fitted results of 900-970 cm^{-1} range, showed that 927 cm^{-1} corresponded to 921 cm^{-1} OH bending vibration in (a). The yellow dotted line is the original spectrum. Raman test conditions: 532 nm laser, range 100-1700 cm^{-1}, test time 8 s, 5 times.

Table 3. The NIR bands and their corresponding MIR peaks. (cm^{-1}).

Sample	Measured peak	Fundamental peaks	Assignments	Theoretical peak	Δ
CT-dio	4125	3443+677	OH stretching vibration + O-Si-O bending vibration	4120	5
	4211	3443+778	OH stretching vibration + Si-O stretching vibration	4221	-10
	4325	3443+886	OH stretching vibration + Si-O stretching vibration	4329	-4
	4700	3018+1681	OH stretching vibration + OH bending vibration	4699	1
	4810	3137+1681	OH stretching vibration + OH bending vibration	4818	-8
	4940	3443+1492	OH stretching vibration + OH bending vibration	4935	5
	5083	3443+1641	OH stretching vibration + OH bending vibration	5084	-1
KQ-mal	4090	3314+776	OH2 stretching vibration + [CO_3] bending vibration	4090	0
	4130	3314+820	OH2 stretching vibration + [CO_3] symmetric stretching vibration ν2	4134	-4
	4168	3402+776	OH1 stretching vibration + [CO_3] bending vibration	4178	-10
	4232	3402+820	OH1 stretching vibration + [CO_3] symmetric stretching vibration ν2	4222	10
	4400	3314+1096	OH2 stretching vibration + [CO_3] stretching vibration ν1	4410	-10
	4508	3402+1096	OH1 stretching vibration + [CO_3] stretching vibration ν1	4498	10
LT-azu	4192	3424+768	OH stretching vibration + [CO_3] stretching vibration	4192	0
	4241	3424+817	OH stretching vibration + [CO_3] symmetric stretching vibration	4241	0

 doi:10.20944/preprints202407.2241.v1

4261	3424+837	OH stretching vibration + [CO_3] antisymmetric stretching vibration	4261	0
4341	3424+921*	OH stretching vibration + OH bending vibration	4245	-4
4373	3424+953	OH stretching vibration + OH bending vibration	4377	-4

* not observed in the spectrum directly. See the analysis for specific reasons.

5. Conclusions

Dioptase exhibits six vibrational bands in the OH stretching vibration region, which are attributed to the vibrations of hydroxyl groups of water molecules with different orientations within the ring silicate structures of the channels. The combination of OH stretching vibrations and Si-O stretching vibrations with the bending vibrations of water molecules results in seven characteristic combination vibration peaks in the near-infrared region of 4000-5200 cm^{-1}. Both malachite and azurite are carbonate minerals. The infrared OH stretching vibration region, ranging between 3000-3500 cm^{-1}, features three types of characteristic peaks: water molecule OH stretching vibrations, structural OH stretching vibrations, and other structural OH stretching vibrations resulting from isomorphous substitution. The near-infrared characteristics appear within the ranges of 4000-4300 and 4300-4500 cm^{-1}, arising from the respective combinations of structural OH stretching vibrations and $[CO_3]^{2-}$ stretching vibrations with OH bending vibrations.

Through the tracing of near-infrared peak positions, a new characteristic peak was identified at 921 cm^{-1} in azurite. Due to its weak intensity and proximity to nearby spectral bands, it has rarely been mentioned before. The combined study of near-infrared and mid-infrared spectroscopy can be used to identify peaks that are difficult to observe in MIR spectroscopy.

Author Contributions: Conceptualization, M.H.; data curation, S.W., S.Y. and S. K.; formal analysis, S.W., M.Y. and B.P.; funding acquisition, M.H.; investigation, M.Y., and B.P.; methodology, S.W. and M.Y.; resources, M.H.; writing—original draft, S.W.; writing—review and editing, S.W., M.Y., B.P., S.Y. and S. K. All authors have read and agreed to the published version of the manuscript.

Funding: Please add: This research was funded by National Mineral Rock and Fossil Specimens Resource Center

Data Availability Statement: Not applicable.

Acknowledgments: In this section, you can acknowledge any support given which is not covered by the author contribution or funding sections. This may include administrative and technical support, or donations in kind (e.g., materials used for experiments).

Conflicts of Interest: The authors declare no conflict of interest.

References

1. Wang, D.H.; Zhang, S.H.; Xiong, X.X.; (Editor in Chief.) Chen, Y.C. (Guidance.) *General Description of Typical Mineral Deposits in the Geological Records of China Volume 1.* Geology Press, Beijing. 2018, p374-437.
2. Tang, Z.Y.; Jiang, Y.; Wang, J.M.; Zhang, M.; Qiao, A.X.; Xiao, L.; Cao, L. Geochemical Characteristics of Rare Earth Elements in Chrysocolla and Dioptase and Their Metallogenetic Environments. *Rock and Mineral Analysis*. **2015**, 34(04): 408-413.
3. Ribbe, P.H.; Gibbs, G.V.; Hamil, M.M. A refinement of the structure of dioptase, $Cu_6[Si_6O_{18}]\cdot 6H_2O$. *American Mineralogist*. **1977**, Vol.62: 807-811.
4. Frost, R.L.; Xi, Y. Thermogravimetric analysis of the copper silicate mineral dioptase $Cu_6[Si_6O_{18}]\cdot 6H_2O$. *Journal of Thermal Analysis and Calorimetry*. **2013**, Vol.112(2): 615-619.
5. Goryainov, S.V. Dehydration-induced changes in the vibrational states of dioptase $Cu_6[Si_6O_{18}]\cdot 6H_2O$. *Journal of Structural Chemistry*. **1996**, Vol. 37(1): 58-64.
6. Ruiz, F.; Martínez, J.R.; González-Hernández, J. Formation of silicate structures in Cu-containing silica xerogels. *Journal of Materials Research*. **2000**, Vol.15(12): 2875-2880.
7. Wang, Y.; Qin, F.; Gao, J.; Qin, S.; Wu, X. In-situ high-pressure X-ray diffraction of natural dioptase. *Acta Petrol. Mineral*. **2015**, 34 (3), 365–370.

8. Qin, F.; Wu, X.; Qin, S.; Zhang, D.Z.; Prakapenka, V.B.; Jacobsen, S.D. Pressure-induced dehydration of dioptase: A single-crystal X-ray diffraction and Raman spectroscopy study. *Comptes Rendus – Geoscience*. **2019**, Vol.351(2): 121-128.
9. Ruan, Q.F.; Song, L.; Yang, Y.; Zhu, S.C.; Bai, F.F. Mineralogical characteristics of dioptase from Kaokoveld, Namibia. *Journal of Guilin University of Technology*. **2016**, Vol.36(2): 223-227.
10. Frost, R.L.; Martens, W.N.; Rintoul, L.; Mahmutagic, E.; Kloprogge, J. T. Raman spectroscopic study of azurite and malachite at 298 and 77 K. *Journal of Raman Spectroscopy*. **2002**, Vol.33(4): 252-259.
11. Yu, B.S.; Fang, J.N.; Huang, E.P. Characteristics of the Raman spectra of archaeological Malachites. *Journal of Raman Spectroscopy*. **2013**, Vol.44(4): 630-636.
12. Jorge-Villar, S.E.; Edwards, H.G.M. Green and blue pigments in Roman wall paintings: A challenge for Raman spectroscopy. *Journal of Raman Spectroscopy*. **2021**, Vol.52(12): 2190-2203.
13. Xu, J.G.; Kuang, Y.Q.; Zhang, B.; Liu, Y.G.; Fan, D.W.; Zhou, W.G.; Xie, H.S. High-pressure study of azurite $Cu_3[CO_3]_2(OH)_2$ by synchrotron radiation X-ray diffraction and Raman spectroscopy. *Physics and Chemistry of Minerals*. **2015**, Vol.42(10): 805-816.
14. Schuiskii, A.V.; Zorina, M.L. Infrared spectra of natural and synthetic malachites. *Journal of Applied Spectroscopy*. **2013**, Vol.80(4): 576-580.
15. Süsse, P. Verfeinerung der Kristallstruktur des Malachits, $Cu_2(OH)_2CO_3$. *Acta Crystallographica*. **1967**, Vol.22(1): 146-151.
16. Belokoneva, E.L.; Gubina, Y.K.; Forsyth, J.B. The charge density distribution and antiferromagnetic properties of azurite $Cu_3[CO_3]_2(OH)_2$. *Physics and Chemistry of Minerals*. **2001**, Vol.28(7): 498-507.
17. Petit, S.; Madejová, J.; Decarreau, A.; Martin, F. Characterization of Octahedral Substitutions in Kaolinites Using Near Infrared Spectroscopy. *Clays and Clay Minerals*. **1999**, 47(1):103-108.
18. Balan, E.; Saitta, A.M.; Mauri, F.; Calas, G. First-principles modeling of the infrared spectrum of kaolinite. *American Mineralogist*. **2001**, 86 (11-12): 1321–1330.
19. Rinnan, Å.; Berg, F.V.D.; Engelsen, S.B. Review of the most common pre-processing techniques for near-infrared spectra. *Trends in Analytical Chemistry*. **2009**, Vol. 28(10): 1201-1222.
20. Medeghini, L.; Mignardi, S.; De Vito, C.; Conte, A.M. Evaluation of a FTIR data pretreatment method for Principal Component Analysis applied to archaeological ceramics. *Microchemical Journal*. **2016**, Vol.125: 224-229.
21. Todorova, M.H.; Atanassova, S.L. Near infrared spectra and soft independent modelling of class analogy for discrimination of Chernozems, Luvisols and Vertisols. *Journal of near infrared spectroscopy*. **2016**, 24(3):271-280.
22. Emsley, J. Very strong hydrogen bonding. *Children & Schools*. **1980**, Vol.9(1): 91-124.
23. Lutz, H.D.; Jung, C. Water molecules and hydroxide ions in condensed materials; correlation of spectroscopic and structural data. *Journal of Molecular Structure*. **1997**, Vol.404(1): 63-66.
24. Werner, M. Stretching frequency versus bond distance correlation of O···D(H)Y (Y = N, O, S, Se, Cl, Br, I) hydrogen bonds in solid hydrates. *Journal of Molecular Structure*. **1986**, Vol.147(1): 1-15.
25. Novak, A. Hydrogen bonding in solids correlation of spectroscopic and crystallographic data. *Large Molecules*. **1974**, Vol.18: 177-216.
26. Libowitzky, E. Correlation of O-H stretching frequencies and O-H···O hydrogen bond lengths in minerals. *Monatshefte fur Chemie*. **1999**, Vol.130(8): 1047-1059.
27. Guo, X.F. Study on Near-infrared Spectra of Silicate Gem Minerals. Kunming University of Science and Technology. 2020.
28. Li X.J.; Zu E.D. Near-Infrared Spectrum Analysis of Cyclosilicates Gem Minerals. *Bulletin of the Chinese Ceramic Society*. **2016**, 35(04): 1318-1321.
29. Stoilova, D.; Koleva, V. Infrared study of some synthetic phases of malachite ($Cu_2(OH)_2CO_3$)—hydrozincite ($Zn_5(OH)_6(CO_3)_2$). *Spectrochimica Acta Part A: Molecular and Biomolecular Spectroscopy*. **2002**, Vol.58(9): 2051-2059.
30. Yang, S.; Gou, Z.N.; Li, P. Analysis of Conventional Gemological Characteristics of Malachite. *China Gems & Jades*. **2021**, Vol.3: 26-30.
31. Farmer, V.C. (Ed.) *The Infrared Spectra of Minerals*; The Mineralogical Society of Great Britain & Ireland: Middlesex, UK, 1974; p268-269.
32. Zheng Y.Y. Spectroscopy Charateristic of Channel Water and Origin Tracing of Dayakou Emerald from Yunan Province. China University of Geosciences (Beijing), 2020.

 doi:10.20944/preprints202407.2241.v1

33. Gao, R.; Chen, Q.L.; Ren, Y.N.; Bao, P.J.; Huang, H.Z. Study on the Gemmological and Spectral Characteristics of Emeralds from Kagem, Zambia. *Spectroscopy and Spectral Analysis*. *2023*, Vol.43(10): 3186-3192.
34. Baron, F.; Petit, S. Interpretation of the infrared spectra of the lizardite-nepouite series in the near- and mid-infrared range. *American Mineralogist*. *2016*, Vol.101: 423–430.
35. Wu, S.K.; He, M.Y.; Yang, M.; Peng, B.J. Near-Infrared Spectroscopic Study of OH Stretching Modes in Kaolinite and Dickite. *Crystals*. *2022*, Vol.12(7): 907.